MINERAL ABUNDANCE, VARIATION, AND COARSENING ACROSS PETROLOGIC TYPES OF H CHONDRITE METEORITES. M. E. Gemma[1,2,3] (mgemma@ldeo.columbia.edu) and D. S. Ebel[2,1,3], [1]Department of Earth and Environmental Science, Columbia University, New York, NY, 10027, [2]Department of Earth and Planetary Sciences, American Museum of Natural History (AMNH), New York, NY, 10024, [3]Lamont-Doherty Earth Observatory, Columbia University, Palisades, NY, 10964.

Introduction: Ordinary chondrite meteorites exhibit mineralogy that is highly variable, dependent on petrologic type [1], and the result of differing parent body processes [2]. Quantifying representative mineralogy in meteorites often involves destructive processes [3, 4] which sacrifice petrographic context in the sample. Furthermore, methods such as point counting do not provide a realistic estimation of modal mineralogy in many chondritic meteorite samples due to their fine-grained nature.

We have examined trends in mineral abundance, variability, and coarsening of opaque assemblages across petrologic types of H chondrite meteorites. By utilizing 2D X-ray element intensity mapping of surfaces to quantitatively determine mineral modal abundances and variability across the petrologic types, we were able to preserve the petrographic context in each sample to assess the phase relationships of opaque assemblages and associated coarsening with petrologic type. This work is part of a broader effort to utilize precise mineral abundances in meteorites to quantitatively link laboratory spectroscopy of meteorites to spectroscopy of asteroids to better understand parent body and asteroid compositions.

Sample Selection: A total of 21 ordinary chondrite falls spanning the full range of petrologic types were sourced from the American Museum of Natural History meteorite collection: nine LL chondrites, eight L chondrites, and four H chondrites. The results for the four H chondrites [Dhajala (H3.8), Buzzard Coulee (H4), Jilin (H5), and Zhovtnevyi (H6)] are reported in this abstract. Complementary work for the LL chondrites was reported in [5], and results of the L chondrite data are forthcoming.

Methods: All samples were first scanned using AMNH's GE phoenix v|tome|x s240 computed tomography scanner to characterize their 3D structure and determine the abundance of opaque (metal and sulfide) phases in approximately 2-6 cm^3 volumes, with resolutions ranging from 6-11 microns/voxel. The CT data was reconstructed to render and process the 3D scan. Next, we were able to calculate the total volume of the sample, isolate mineral phases based on density, and choose an appropriate area to cut for 2D chemical analysis. Each sample was then cut and polished to create a thick or thin section of the meteorite. These sections were subsequently mapped using AMNH's Cameca SX5-Tactis Electron Microprobe for the X-ray intensities of ten major and minor elements (Mg, Si, Ca, Al, Fe, Ni, S, Ti, Cr, and P) at a resolution of 4 microns/pixel, over a sufficient area (~1 cm^2) to characterize mineralogy in a 2D slice (**Fig. 1**, left). Red-Green-Blue (RGB) composite images, using one element map in each color channel (Red = Fe, Green = Ni, Blue = S), were used to qualitatively evaluate mineral diversity (**Fig. 1**, right).

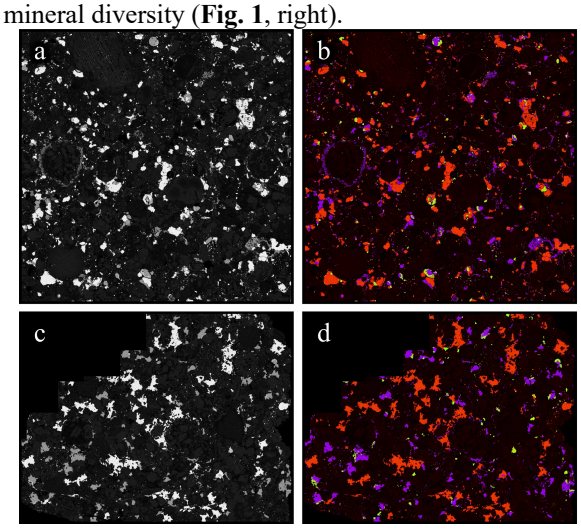

Figure 1: a) X-ray element intensity map of Fe in a thin polished section of Dhajala (H3.8). Brighter areas represent higher abundances of Fe. c) X-ray element intensity map of Fe in a thick polished section of Jilin (H5). b,d) RGB composite images of mapped Dhajala section (*b*, Dimensions = 0.6144 cm x 0.6144 cm) and Jilin section (*d*, Dimensions = 0.8192 cm x 0.6144 cm). Red = Fe, Green = Ni, Blue = S. Mixed phases in images correspond to kamacite (orange), taenite (green), and troilite (purple).

In order to quantitatively address mineral diversity, acquired element maps were linearly combined to determine the mineralogy of each individual pixel in a map. This enabled calculation of the relative mineral abundances in each meteorite [6] (**Fig. 2, Table 1**). Metal and sulfide abundances determined from 3D data can be used as a check against the 2D modal abundance map (**Fig. 2**) to ensure that the 2D section is representative. The higher percentage of "unknown" pixels found in Dhajala (H3.8) and Buzzard Coulee (H4) is expected due the fine grained nature of the sample. The lower number of "unknown" pixels for the samples of higher petrologic grade, Jilin (H5) and Zhovtnevyi (H6) can be attributed to the coarser nature of the various mineral phases.

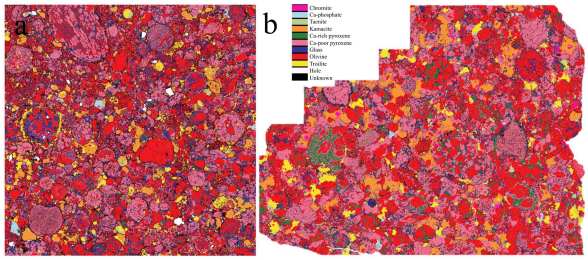

Figure 2: Mineral modal abundance map of a) Dhajala (H3.8), Dimensions = 0.6144 cm x 0.6144 cm, and b) Jilin (H5), Dimensions = 0.8192 cm x 0.6144 cm. Each pixel was assigned a mineral phase using linear combinations of the element maps.

Mineral Phase	Dhajala (H3.8)	Buzzard Coulee (H4)	Jilin (H5)	Zhovtnevyi (H6)
Olivine	31.40%	36.11%	34.65%	35.90%
Ca-poor pyroxene	24.53%	26.62%	30.82%	32.67%
Glass	13.01%	4.25%	7.35%	10.20%
Ca-rich pyroxene	2.70%	5.80%	5.50%	5.80%
Troilite	4.31%	7.18%	4.45%	4.27%
Ca-phosphate	0.73%	0.54%	0.35%	0.64%
Kamacite	5.28%	7.34%	6.54%	3.43%
Taenite	1.13%	1.52%	0.89%	0.90%
Chromite	0.35%	0.73%	0.61%	0.45%
Unknown	16.56%	9.91%	8.84%	5.74%
*Metal	6.41%	8.86%	7.43%	4.33%
+Opaques	10.72%	16.04%	11.88%	8.60%

Table 1: Mineral Modal Abundances of H Chondrite samples from each petrologic type (3-6). *Metal: kamacite and taenite values added together. +Opaques: kamacite, taenite, and troilite (FeS) values.

Results/Discussion: We demonstrated in [5] for a suite of LL chondrite samples that 2D element mapping of a ~1 cm^2 sample surface area produces mineral abundances consistent with 3D bulk scans of a ~4 cm^3 parent sample. Abundances of mineral phases in 2D and 3D were consistent to within 1% for equilibrated LL samples (petrologic types 4-6), and generally to within ~2% for the unequilibrated LL samples (petrologic type 3). The larger inconsistencies observed in the 2D and 3D abundances for the unequilibrated LL samples was likely due to the more heterogeneous nature of the unequilibrated meteorites. We find similar results for the H chondrite samples analyzed here (**Fig. 2, Table 1**). Upcoming work will include mapping multiple sections from a single unequilibrated ordinary chondrite to evaluate the effects of heterogeneity (or lack thereof) on 2D vs. 3D abundances. The calculated mineral modal abundances support the conclusion from [5] that 2D mapping of an area ~0.6 cm^2 - 1 cm^2 is representative of the bulk meteorite sample, at least for the major mineral phases. Calculated mineral abundances for the H chondrite samples are also broadly consistent with existing literature on the compositions of ordinary chondrites [3,4,7,8].

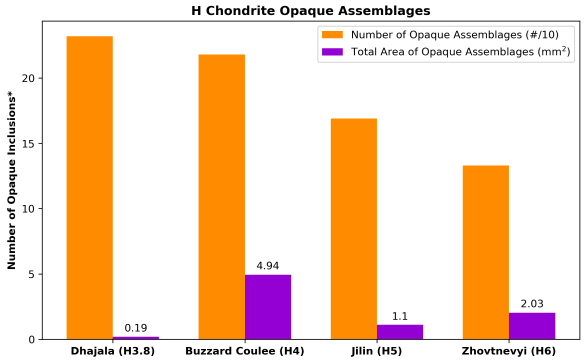

Figure 3: Comparison of number vs. area of opaque assemblages across petrologic type for the H chondrites. The total number of opaque assemblages for each meteorite (y-axis) was divided by ten to enable better graphic representation.

Coarsening of opaque assemblages (metal + sulfide phases) with increasing petrologic grade is apparent in Figure 3, which compares the total area of the opaque assemblages to the number of opaque assemblage inclusions in each meteorite. The number of opaque assemblages decreases as petrologic grade increases, accompanied by a general increase in total area of the opaque assemblages. Buzzard Coulee (H4) appears to be an outlier in the trend due to its noticeably larger Fe abundance (Table 1). Additionally, the total opaque assemblage abundances in Table 1 appear to broadly decrease with increasing petrologic type. This is likely due to undersampling of the coarsened (larger) opaque phases in the 2D area we measured. Comparing a larger mapped area of the samples of higher petrologic type to the mapped areas reported here will confirm or deny this.

Acknowledgments: The authors thank the staff at the AMNH EPMA facility for operational assistance. This work was supported by NASA Emerging Worlds grant NNX16AD37G (DE).

References: [1] McSween H. et al. (1991) Icarus, **90**, 107–116. [2] Jones R. H., et al. (2014) Geochim. Cosmochim. Acta **132**, 120–140. [3] Dunn T. et al. (2010) Meteor. Planet. Sci. **45**, 123-134. [4] Menzies O. et al. (2005) Meteor. Planet. Sci. **40**, 1023-1042. [5] Gemma M.E. and Ebel D.S. (2002) *LPSC LI,* Abstract #2588. [6] Crapster-Pregont, E. J. and Ebel, D. S. (2020) Microscopy and Microanalysis, **26**, 63-75. [7] Gastineau-Lyons H. et al. (2002) Meteor. Planet. Sci. **37**, 75-89. [8] Weisberg M. et al. (2006) Meteorites and the Early Solar System, 19-52.